

## Chapter 6

# Coupling-current losses in accelerator dipole magnets

*This chapter deals with the losses during ramping in superconducting magnets and in particular in the LHC-type dipole magnets. The filament magnetisation, the coupling loss in the wedges and the resistive loss are briefly discussed.*

*The interfilament coupling loss (IFCL) is analysed as a function of the central-field-sweep rate, the time constant of the interfilament coupling currents and a geometry factor that expresses the field variation over the cross-section of the coil.*

*In a similar way, the interstrand coupling loss (ISCL) is investigated as a function of the field-sweep rate, the cross-contact resistance and a geometry factor that denotes the ratio between the local field normal to the cable width and the central field. The increase of the average time constant of the ISCCs in a coil as compared to a single cable is dealt with as well. The ratio between the time constant and the coupling power loss is investigated for several variations of the cross-contact resistance over the cross-section of the coils.*

*Characteristic values for the loss of LHC dipole magnets are given in the case of a nominal field cycle and the distribution of the various loss components over the cross-section of the coils is illustrated.*

*Experimental results are presented of the losses during ramping in 11 LHC dipole model magnets, with lengths of 1 and 10 m. The losses are determined as the difference between the stored energy and the extracted energy during field sweeps between 0.02 and 0.2 Ts<sup>-1</sup>. Differences in the coupling loss among the various model magnets are explained by means of different contact resistances.*

## 6.1 Introduction

During charging and discharging of superconducting magnets energy is dissipated through several mechanisms. The main contributions are due to the magnetisation of the superconducting filaments, the interstrand coupling currents (ISCCs), the interfilament coupling currents (IFCCs) and the resistive loss in the cable-to-cable connections. Smaller contributions originate from the magnetisation of the iron yoke and the eddy currents in the copper wedges and collars.

The induced coupling currents not only cause energy loss but they also cause field distortions and reduce the temperature margin of the coil during (de-)excitation. A good understanding of the loss components is therefore important as they have a major impact on the installed cryogenic power, the allowable excitation ramp-rate, the electromagnetic stability and the quench-protection scheme.

In section 6.2 the various loss components are discussed.

The filament magnetisation and the IFCL are qualitatively treated by means of the theory presented in chapter 3. Representative values of the losses during ramping in LHC dipole magnets are made, using the experimental results on short pieces of LHC-type cables (see sections 3.3 and 3.5). The field shape over the cross-section of the coils is expressed by a field geometry factor  $\beta_{str}$  which is defined as the local field at the strand divided by the central field of the magnet.

The ISCL in a coil is calculated by modelling the turns of the coil by means of a network of nodes interconnected by strand sections and contact resistances  $R_c$  as discussed in detail in chapter 4. The turns of the coil are subject to the local field variation and the mutual interaction between the ISCCs of all the turns is taken into account. The ISCL depends mainly on the field change  $\dot{B}_\perp$  normal to the cable width and is expressed as a function of the average contact resistance  $R_c$  of the cable. The ratio between the perpendicular field component and the central field is expressed by the factor  $\beta_p$ . The enhancement of the coupling loss, due to the boundary-induced coupling currents (see chapter 5), is disregarded since the exact increase is hard to calculate but is at least one order of magnitude smaller than the total coupling loss.

The ratio between the ISCL of a magnet and the average time constant  $\tau_{is,M}$  of the ISCCs is investigated for various  $R_c$ -distributions over the blocks of the inner coil. A good understanding of the time constants is essential to evaluate time-dependent effects in magnets.

In section 6.3 the method is described by which the losses during ramping of the LHC dipole model magnets are measured. The method is based on the electrical measurement of the stored energy during excitation of the coil and the extracted energy during de-excitation. The advantages of the electrical method as compared to other measurement techniques are discussed.

In section 6.4 the experimental results of the losses during ramping of 11 LHC dipole model magnets are presented. The hysteresis loss is compared to the calculated values. The coupling-current loss is presented by means of average  $R_c$ -values. The results are used to evaluate:

- The expected energy loss during ‘normal’ excitation of the LHC dipole magnets, and during a fast de-excitation (in the case a quench occurred in a series connected magnet).

- The difference between the  $R_c$ -values of the two apertures and four poles of a twin-aperture magnet. Large differences imply that the  $R_c$ -distribution over the cross-section of the coil could vary strongly, which in turn enhances the field distortions caused by the coupling currents (see chapter 7).
- The  $R_c$ -values of similar cables that are used in different magnets.

Furthermore, quantitative knowledge of the average  $R_c$  of the various magnets is necessary to correlate:

- the ramp-rate induced field errors with the ISCCs, as discussed in chapter 7,
- the ramp-rate limitation of the quench current with the ISCCs and the ISCL, as discussed in chapter 8.

## 6.2 Loss components in magnets

In chapters 3 and 4 the losses at strand and cable levels are dealt with in detail. In this section the losses at magnet level are discussed. The calculations are based upon the formulas obtained in the above-mentioned chapters, taking into account the geometry of the magnet and the interaction between the turns. The characteristic power-loss distribution over the cross-section of the coils is illustrated, using the experimentally determined values for the  $J_c$ - $B$  relation (see section 3.3), the interfilament time constant  $\tau_{if}$  (see section 3.5) and the cross-contact resistance  $R_c$  (see section 4.10).

The losses in the mechanical structure are not dealt with in detail but are calculated to be small compared to the other loss components.

The eddy-current loss in the collar pieces of the LHC dipole magnets is small since they consist of separate aluminium or stainless steel plates of 5 mm thickness. The energy loss is about 0.4 J during excitation and 3 J during a fast de-excitation in a 1 m long twin-aperture magnet, assuming a resistivity of the collars of  $10^{-9}$   $\Omega\text{m}$ . This is smaller than 1% of the total losses during (dis)charging (see Table 6.2).

The magnetisation loss in the iron yoke is estimated to be about 40 mJ per kg iron for a field cycle between 0 and 1.7 T [Andreyev, '85]. In the case of a 1 m long twin-aperture magnet, this implies a loss of about 20 J for a nominal field sweep between 0.5 and 8.4 T. This is about 10% of the expected hysteresis loss in the filaments (assuming a filament diameter of 5  $\mu\text{m}$ ) of about 200 J per metre (see Table 6.2).

The mechanical work of the coils due to their deformation during a field sweep is disregarded.

In sections 6.2.1-6.2.4 the field variation in the coil ends is disregarded and the turns are considered to be infinitely long. The enhancement of the loss due to the BICCs is not taken into account.

### 6.2.1 Hysteresis loss

The hysteresis loss  $Q_{hys}$  in the superconducting filaments has already been dealt with in section 3.2. Here full penetration of the filaments is assumed, which is usually the case in high-field accelerator magnets because the field is much larger than the penetration field.

The hysteresis loss (per unit volume) of the filaments for a field cycle with a small field-sweep rate  $\dot{B}$  is given by eq. 3.8 (at constant temperature):

$$Q_{hys} = \frac{2d_f}{3\pi} \oint J_C(B) \left( 1 + (I_{tr}/I_C(B))^2 \right) \left| \dot{B}_{\perp f} \right| dt \quad [\text{Jm}^{-3}/\text{cycle}], \quad (6.1)$$

where  $B_{\perp f}$  denotes the local field perpendicular to the filament axis. The relation between the critical current and the field is given by eqs. 2.16 and 2.17 (or 2.18). A possible interaction between the filaments of the strand is included in the  $I_C$ - $B$  relation since experimental results are usually obtained on a strand and not on single filaments. The hysteresis loss depends on the initial and final field values of the cycle and, for low  $\dot{B}$ , not on the field-sweep rate. The hysteresis loss in the coil ends is not treated here but can be calculated in exactly the same way by taking into account the field distribution in the ends.

In section 3.5 it is concluded that for small  $\dot{B}$  and high fields (compared to the penetration field) the hysteresis loss of a single strand is not affected by the other strands of the cable. This also implies that the hysteresis loss in each turn of a coil is not significantly affected by the other turns. The hysteresis loss  $Q_{hys,i}$  of turn  $i$  is therefore equal to the sum of the hysteresis losses of all the strands in the cable subject to the local field. Likewise, the hysteresis loss of the magnet is determined by the sum of the hysteresis loss of all the turns. The average field  $B_{\perp f}$  of all the filaments in a strand is expressed by the field  $B_{str}$ . Since the local field  $B_{str}$  of each strand varies, it is convenient to write the loss as a function of the central field  $B_{ce}$ . The field geometry factors  $\beta_{str,i,j}$  relate the field  $B_{str,i,j}$  at turn  $i$  and strand position  $j$  to the central field:

$$B_{str,i,j} = \beta_{str,i,j} B_{ce} \quad [\text{T}]. \quad (6.2)$$

The total hysteresis loss of a coil during a field sweep  $B_{ce,1}$ - $B_{ce,2}$ - $B_{ce,1}$  (at constant temperature) can then be written as:

$$E_{hys,coil} = f(d_f, I_C(B), I_{tr}, \beta_{str,i,j}, B_{ce,1}, B_{ce,2}) \quad [\text{J}]. \quad (6.3)$$

The coils of multishell magnets are usually made of different cables (in order to obtain a good grading of the current density) with a different  $I_C$ - $B$  relation and possibly a different filament diameter. The hysteresis loss of each coil is therefore expressed by a relation of the form of eq. 6.3. Quantitative results of the hysteresis loss of LHC dipole magnets for a nominal operation cycle are given in section 6.2.5.

### 6.2.2 Interfilament coupling loss

The power loss density  $P_{if}$  in strands with a round or square cross-section in a ramped field is given by (combining eqs. 3.15 and 3.20):

$$P_{if} = \frac{2\tau_{if}}{\mu_0} \dot{B}_{\perp s}^2 \quad [\text{Wm}^{-3}], \quad (6.4)$$

with  $B_{\perp s}$  the field perpendicular to the strand axis. Eq. 6.4 is valid as long as the field is large compared to the penetration field and the filaments are not saturated.

In section 3.5 it is concluded that for small frequencies and large fields (compared to the penetration field) the IFCL of a single strand is not influenced by the other strands of the cable. This also implies that the IFCL of a single turn of a coil is not affected by the neighbouring turns so that the coupling power loss  $P_{if,i}$  of turn  $i$  in a coil is equal to the sum of the power losses of all the individual strands  $j$  in the turn (subject to the local field change  $\dot{B}_{str,i,j}$ ). The IFCL of turn  $i$  for one aperture of length  $l_M$  (disregarding the ends) can then be expressed as a function of the central-field-sweep rate  $\dot{B}_{ce}$ :

$$P_{if,i} = \frac{2\tau_{if,i}}{\mu_0} V_i \beta_{str,i}^2 \dot{B}_{ce}^2 \quad [\text{W}], \quad (6.5)$$

with:

$$V_i = 4whp_{cab}l_M \quad [\text{m}^3], \quad (6.6)$$

the volume of turn  $i$ ,  $p_{cab}$  the packing factor of the cable (about 0.9) and:

$$\beta_{str,i}^2 = \frac{1}{N_s} \sum_{j=1}^{N_s} \beta_{str,i,j}^2. \quad (6.7)$$

The factor 4 in eq. 6.6 refers to the four quadrants of an aperture. Note that  $w$ ,  $h$  and  $p_{cab}$  can be different for the various coils of a multishell magnet.

The  $(\beta_{str,i})^2$ -values are shown in Fig. 6.1 for two dipole-magnet geometries. The IFCL is mainly generated in the inner coil and near the pole of the outer coil. The IFCL in a block and in the coil are equal to the sum of the losses of the individual turns in the block and coil respectively. The IFCL during a nominal field sweep is given in section 6.2.5.

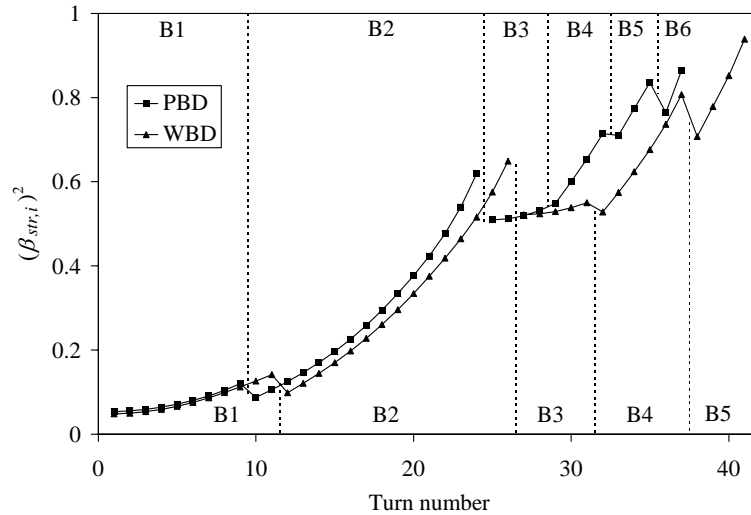


**Figure 6.1.** The field geometry factor  $(\beta_{str,i})^2$  for each turn of the PBD and WBD magnets (see Table 2.1). The labels B1-B6 at the top and B1-B5 at the bottom refer to the blocks of the PBD and WBD designs respectively (see Fig. 2.2b).

### 6.2.3 Interstrand coupling loss

The steady-state ISCL of a cable, subject to a transverse field change, is dealt with in detail in section 4.4.1. Here the increase of the ISCL due to the spatial distribution of  $\hat{B}_\perp$  along the cable length as well as the coupling loss in the resistances  $R_a$  are disregarded. According to eq. 4.17, the coupling power loss  $P_{c,i}$  per turn can then be written as:

$$P_{c,i} = 8.49 \cdot 10^{-3} \frac{L_{p,s} w^2 (N_s^2 - N_s)}{R_{c,i}} 4l_M \beta_{p,i}^2 \dot{B}_{ce}^2 \quad [\text{W}], \quad (6.8)$$

with  $R_{c,i}$  the average  $R_c$  of turn  $i$ . The factor  $4l_M$  is introduced since the ISCL in eq. 4.17 is given per unit length of cable while the ISCL in eq. 6.8 is given for one aperture of length  $l_M$  which consists of four quadrants.

The factors  $\beta_{p,i}$  are the field geometry factors that express the ratio between the local effective transverse field of turn  $i$  and the central field. Variations of  $\hat{B}_\perp$  across the cable width that affect the coupling power loss (see section 4.7), are incorporated in the factors  $\beta_{p,i}$ . The factors  $(\beta_{p,i})^2$  for each turn of the PBD and WBD magnets are shown in Fig. 6.2.

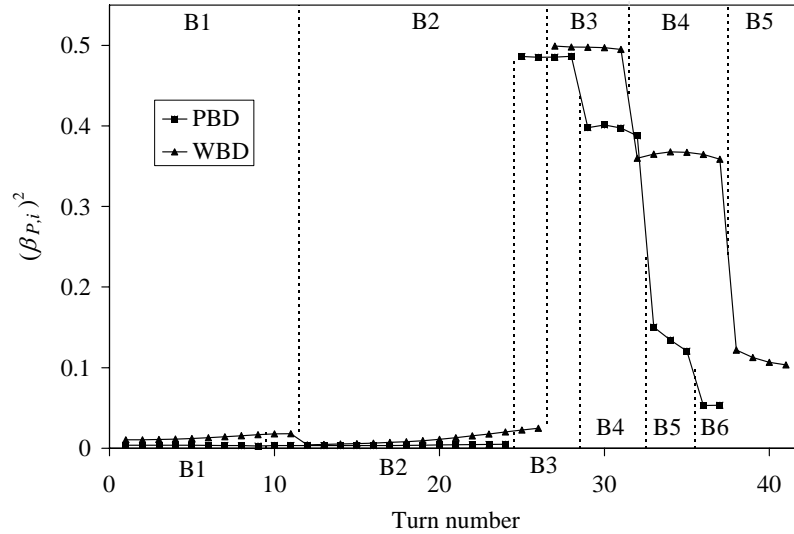


**Figure 6.2.** The field geometry factor  $(\beta_{p,i})^2$  for each turn of the PBD and WBD magnets (see Table 2.1). The labels B1-B6 at the bottom and B1-B5 at the top refer to the blocks of the PBD and WBD designs (see Fig. 2.2b) respectively.

The ISCL is mainly generated in the inner coil (B3-B6 for the PBD magnet and B3-B5 for the WBD magnet) and especially in the turns close to the midplane due to the large field component perpendicular to the cable width (assuming similar cable pitches and contact resistances of the inner and outer coils). Note that  $\beta_p$  is very small near the midplane of the outer coil (B1) because  $\hat{B}_\perp$  changes sign which results in a very small ISCL (see Fig. 4.17).

The steady-state ISCL of the coil is obtained by summation of the ISCL over all the turns. A first estimate of the ISCL for an arbitrary coil wound from Rutherford-type cables can be easily obtained using eq. 6.8 where the factors  $\beta_{p,i}$  are calculated by taking the field component normal to the cable width of turn  $i$  in the centre of the cable. In the case of a cable with  $R_a \ll R_c$  eq. 6.8 has to be extended with the power loss  $P_a$  in the resistances  $R_a$  given by eq. 4.16. Note that different field geometry factors have to be used for  $P_a$  that express the ratio between the local effective parallel field and the central field.

Due to the mutual interaction between the ISCCs of the various turns, the average time constant  $\tau_{is,M}$  of the ISCCs in a magnet will be considerably larger than the average time constant  $\tau_{is,cab}$  of the ISCCs in a single cable (see also section 4.9). The time constant  $\tau_{is,M}$  is numerically calculated using the network model where the mutual inductances between all the strands of the various turns are incorporated. The influence of the ISCCs of the outer coil is disregarded in order to limit the computing time. This results in an error in the calculated  $\tau_{is,M}$  of less than 5% if the  $R_c$ -values and cable pitches of the inner and outer coils are equal.

The mean time constant of the ISCCs in a magnet is then proportional to the time constant  $\tau_{is,cab}$  of the ISCCs in the cable of the inner coil (see eq. 4.31):

$$\tau_{is,M} = K \tau_{is,cab} \quad [\text{s}] . \quad (6.9)$$

The constant of proportionality  $K$  depends on the magnet geometry and is equal to 4.5 for the PBD magnet and 4.3 for the WBD magnet (both values with an error of about 10%). Also for other coil configurations, such as the HERA- and the SSC-dipole geometries the factor  $K$  will be about 4-5. The factor  $K$  can be roughly approximated by calculating the ratio  $\tau_{is,M}/\tau_{is,cab}$  using eq. 4.41 taking  $\alpha_{cab}=7.5$  and  $N_c=16$  and assuming  $\tau_{is,M} = \tau_{is,st}$ . The number  $N_c=16$  is used since the ISCL in a dipole coil is mainly generated in B3 and B4 which form a stack of 16 cables (for the PBD magnet) for quadrants 1 and 4 or 2 and 3 (see Fig. 2.2b). The factor  $K$  is somewhat smaller than the calculated ratio  $\tau_{is,M}/\tau_{is,cab}=5$  due to the presence of a wedge between blocks 3 and 4.

It is shown in section 4.9 that, for a given field-sweep rate, the ratio  $\tau_{is,st}/P_c$  is almost independent of the  $R_c$ -distribution among the cable pieces (up to differences of a factor 5). Here the ratio between the average time constant of the magnet  $\tau_{is,M}$  and the coupling power loss  $P_{c,M}$  is investigated by systematically varying  $R_c$  over the four blocks of the inner coil of the PBD magnet (see Table 6.1).

Note that these values cannot be easily correlated to the results given in Table 4.3 since the field change is not constant over the cross-section of the coils. The given time constants are average values for the blocks or the magnet, since in an actual coil, the current  $I_s$  in each strand section of each turn has its own time constant. The factor  $\tau_{is,M}/P_{c,M}$  is almost independent of the  $R_c$ -distribution even though  $R_c$  is varied by a factor of 5. This is caused by the presence of the wedges which decrease the mutual inductances between the blocks which can therefore be regarded as independent parts. This can be easily seen in Table 6.1 where a decrease of  $R_c$  in one block does not affect the time constants of the other blocks.

**Table 6.1.** Average time constants of the ISCCs in the four blocks B3, B4, B5 and B6 and in the whole PBD magnet M, and total coupling power loss (for one aperture with a length of 1 m) for various  $R_c$ -distributions over the four blocks ( $\dot{B}_{ce}=0.066 \text{ Ts}^{-1}$ ,  $L_{ps}=0.1 \text{ m}$ ,  $N_s=26$ ).

$R_c$ ( $\mu\Omega$ )				$\tau_{is,av}$ (s)				$\tau_{is,M}$	$P_{c,M}$	$\tau_{is,M}/P_{c,M}$
B3	B4	B5	B6	B3	B4	B5	B6	(s)	(W)	( $\text{sW}^{-1}$ )
10	10	10	10	0.46	0.39	0.47	0.30	0.42	1.14	0.37
2	10	10	10	2.02	0.42	0.48	0.31	1.32	3.50	0.38
10	2	10	10	0.46	1.74	0.55	0.31	1.06	2.86	0.37
10	10	2	10	0.45	0.40	2.00	0.33	0.58	1.53	0.38
10	10	10	2	0.46	0.39	0.48	1.27	0.46	1.23	0.37

Variations of  $R_c$  within a block lead to variations of the ratio  $\tau_{is}/P_c$  within the block (as already discussed in section 4.9), and so to variations of  $\tau_{is,M}/P_{c,M}$ . For large  $R_c$ -variations of a factor of 10 within one block, the ratio  $\tau_{is,M}/P_{c,M}$  can change by an average of 10%.

Hence, it can be concluded that, if the power loss is known, the time constant can be deduced (and conversely) for an arbitrary  $R_c$ -distribution over the blocks and within the blocks, with an accuracy of about 10% for  $R_c$ -variations up to a factor of 10. This implies that the decay of the voltage over a magnet after a field sweep gives the ISCL and therefore the average  $R_c$  (if the regulation of the current supply is perfect). However, no information is obtained about the other loss components of the magnet such as the resistive loss and the hysteresis loss.

#### 6.2.4 Losses in the connections and the wedges

In the resistive cable-to-cable connections between the poles and the coils an ohmic loss power:

$$P_R = I^2 R_{tot} \quad [\text{W}], \quad (6.10)$$

is generated, where  $R_{tot}$  denotes the sum of the resistances of all cable-to-cable connections in the magnet (see section 2.2). Note that the resistances, and therefore the power  $P_R$ , depend on the field due to the magnetoresistance and possibly slightly on the current and the field-sweep rate. A good approximation of the resistive loss for a given field cycle is obtained by integration of eq. 6.10 using a value of the resistance at the mean field level (see section 6.2.5).

The eddy-current power loss in the copper wedges  $P_{wed}$  of one aperture is inversely proportional to the resistivity  $\rho_{cu}$  of copper and proportional to  $\dot{B}_{ce}^2$  and satisfies:

$$P_{wed} = \frac{C_{wed} l_M}{\rho_{cu}(B)} \dot{B}_{ce}^2 \quad [\text{W}], \quad (6.11)$$

where  $C_{wed}$  depends on the number and geometry of the wedges and the field distribution over the cross-section of the wedges. Taking one aperture of the PBD magnet,  $C_{wed}$  is about  $3 \cdot 10^{-8} \text{ m}^4$ , so that  $P_{wed}$  is about 7 mW for  $\rho_{cu}=4 \cdot 10^{-10} \text{ }\Omega\text{m}$  and  $\dot{B}_{ce}=0.01 \text{ Ts}^{-1}$ .

The energy losses in the connections and the wedges during a nominal field sweep are given in the next section.

### 6.2.5 Total loss

The energy loss of one aperture of a magnet of length  $l_M$  during a triangular field cycle  $B_{ce,1}$ - $B_{ce,2}$ - $B_{ce,1}$  (with  $B_{ce,2} > B_{ce,1}$ ) with constant field-sweep rate  $\dot{B}_{ce}$  is determined by integration of eqs. 6.5, 6.8, 6.10 and 6.11:

$$Q_{tot} = Q_{hys} + \sum_{i=1}^{N_T} \left( \oint P_{if,i} dt + \oint P_{is,i} dt \right) + \oint P_R dt + \oint P_{wed} dt \quad [\text{J/cycle}], \quad (6.12)$$

with:

$$\oint P_{if,i} dt = \frac{2\tau_{if}}{\mu_0} (4whp_{cab} l_M) 2\beta_{str,i}^2 \left[ (B_{ce,2} - B_{ce,1}) \dot{B}_{ce} - \tau_{if} \dot{B}_{ce}^2 \right] \quad [\text{J/cycle}], \quad (6.13)$$

$$\begin{aligned} \oint P_{is,i} dt = 8.49 \cdot 10^{-3} \frac{L_{p,s} w^2 (N_s^2 - N_s)}{R_{c,i}} 4l_M \beta_{p,i}^2 * \\ 2 \left[ (B_{ce,2} - B_{ce,1}) \dot{B}_{ce} - \tau_{is,M} \dot{B}_{ce}^2 \right] \quad [\text{J/cycle}], \end{aligned} \quad (6.14)$$

and:

$$\oint P_R dt = \oint \frac{B_{ce}^2 R_{tot}}{T_M^2} dt = \oint \frac{B_{ce}^2 R_{tot}}{T_M^2} \frac{1}{\dot{B}_{ce}} dB_{ce} = \frac{2R_{tot}}{3T_M^2 \dot{B}_{ce}} (B_{ce,2}^3 - B_{ce,1}^3) \quad [\text{J/cycle}], \quad (6.15)$$

with  $N_T$  the number of turns in the coils and  $T_M$  [ $\text{TA}^{-1}$ ] the field factor of the magnet. The loss contributions in the iron yoke and the collars are disregarded here.

Measurements of losses during ramping are usually performed with ramp times (from  $B_{ce,1}$  to  $B_{ce,2}$  and reversely) of the order of  $10^1$ - $10^3$  s. The term  $\tau_{if} \dot{B}_{ce}^2$  in eq. 6.13 can therefore be neglected since the time constant  $\tau_{if}$  (which is of the order of 10-100 ms, see section 3.5) is much smaller than the ramp time. The term  $\tau_{is,M} \dot{B}_{ce}^2$  in eq. 6.14 should be taken into account for small ramp times since  $\tau_{is,M}$  is of the order of 1-10 s for LHC-type cables (see section 6.4).

The energy loss in the wedges depends on the relation between the resistivity of the copper and the magnetic field. A simple expression can be used to estimate the loss by assuming a field-independent resistivity which is equal to the resistivity of the copper at a field  $(B_{ce,2} + B_{ce,1})/2$ , so that:

$$\oint P_{wed} dt = 2 \frac{C_{wed} l_M}{\rho_{cu}} (B_{ce,2} - B_{ce,1}) \dot{B}_{ce} \quad [\text{J/cycle}]. \quad (6.16)$$

The ISCL, the IFCL and the hysteresis loss of one aperture of a PBD magnet are depicted in Fig. 6.3. The resistive loss in the connections is not shown since the loss is locally dissipated. The losses are calculated for a field cycle between 0 and 2 T and are depicted for each turn individually. This cycle is chosen as it is often applied in the loss measurements during ramping (see section 6.4).

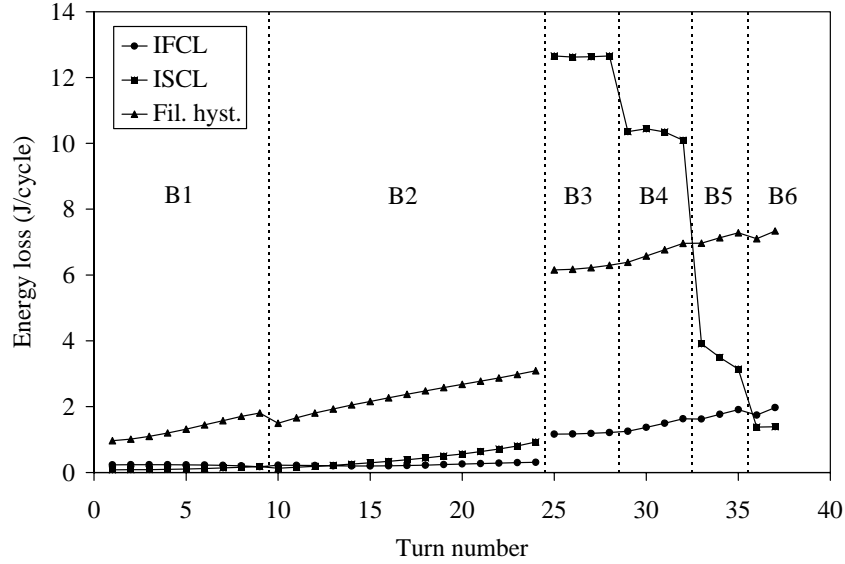


**Figure 6.3.** The hysteresis loss, IFCL and ISCL for each turn of the straight part of one aperture of a 1 m long PBD magnet (see Fig. 2.b2 for the numbering of the turns and the blocks). The loss is calculated for a field cycle between 0 and 2 T with  $\dot{B}_{ce}=0.1 \text{ Ts}^{-1}$ ,  $R_c=10 \mu\Omega$ ,  $L_{p,s}=0.10 \text{ m}$ ,  $B_0=0.31 \text{ T}$ ,  $J_0=3.2 \cdot 10^{10} \text{ Am}^{-2}$ ,  $d_f=10 \mu\text{m}$  and  $\tau_{if}=25 \text{ ms}$ .

The losses in the strand are based on the experimental results of an LHC-type cable with  $B_0=0.31 \text{ T}$ ,  $J_0=3.2 \cdot 10^{10} \text{ Am}^{-2}$ ,  $d_f=10 \mu\text{m}$  and  $\tau_{if}=25 \text{ ms}$  (see chapter 3). The contact resistance  $R_c$  is taken as  $10 \mu\Omega$ . Note that:

- the hysteresis loss increases near the pole of the magnet where the field is maximum,
- the hysteresis loss in the outer coil is relatively large compared to the coupling losses since the hysteresis loss is mainly generated at small fields where the critical current density is large,

the IFCL in the LHC dipole magnets is about 5 times smaller than the ISCL for  $R_c=10 \mu\Omega$  and  $\tau_{if}=25 \text{ ms}$ . A survey of the various loss components during a nominal field sweep of the PBD and WBD magnets is given in Table 6.2. The IFCL and the ISCL are calculated using eqs. 6.13 and 6.14 with:

$$\sum_{i=1}^{N_T} \beta_{str,i}^2 = 5.1 + 8.5 = 13.6, \quad (6.17)$$

and:

$$\sum_{i=1}^{N_T} \beta_{p,i}^2 = 0.09 + 4.04 = 4.13, \quad (6.18)$$

where the two numbers indicate the summations over the turns of the outer and the inner coil respectively.

**Table 6.2.** The energy loss of the various components for a nominal field sweep between 0.6 and 8.4 T with  $\dot{B}_{ce}=0.0066 \text{ Ts}^{-1}$  and a fast exponential de-excitation with a time constant  $\tau_d=100 \text{ s}$  for the PBD and WBD magnets at 1.9 K. The losses are given per metre for a twin-aperture magnet.  $R_c=2 \mu\Omega$ ,  $\tau_{ij}=25 \text{ ms}$ ,  $L_{p,s}=0.12 \text{ m}$ . The ISCL is inversely proportional to  $R_c$ . The filament diameter is  $5 \mu\text{m}$  for both magnets.

	Excitation: $0.0066 \text{ Ts}^{-1}$		Fast de-excitation: $\tau_d=100 \text{ s}$	
	PBD	WBD	PBD	WBD
Hysteresis loss (J)	210	200	210	200
IFCL (J)	7	6	46	42
ISCL (J)	170	210	1150	1390
Resistive loss (J)	38	26	4.1	2.8
Loss in the wedges <sup>a</sup> (J)	1.2	1.1	8	7
Loss in the collars <sup>b</sup> (J)	0.4	0.4	3	3
Loss in the iron yoke <sup>c</sup> (J)	20	20	20	20
Total (J)	450	460	1440	1660
Average heat load (W)	0.38	0.39	14.4	16.6

<sup>a</sup> assuming a resistivity that linearly increases from  $2 \cdot 10^{-10} \Omega\text{m}$  at 0.6 T to  $10 \cdot 10^{-10} \Omega\text{m}$  at 8.4 T.

<sup>b</sup> an estimate assuming a resistivity of the collars of  $10^{-9} \Omega\text{m}$ .

<sup>c</sup> an estimate assuming a loss of 20 mJ per kg iron for a mean field sweep in the yoke from 0 to 1.7 T.

The hysteresis loss is calculated using the  $I_C$ - $B$  relations described by eqs. 2.16 and 2.18 with  $B_0=0.31 \text{ T}$ ,  $J_0=3.2 \cdot 10^{10} \text{ Am}^{-2}$ ,  $C_1=112 \cdot 10^3 \text{ A}$ ,  $C_2=7.8 \cdot 10^3 \text{ AT}^{-1}$  and  $T=1.9 \text{ K}$ .

The resistive loss is the loss for one twin-aperture magnet and is calculated for four splices (each with a resistance that linearly increases from  $0.3 \text{ n}\Omega$  at 0.6 T to  $1.5 \text{ n}\Omega$  at 8.4 T) and three pole-to-pole connections (with a constant resistance of  $0.2 \text{ n}\Omega$ ). Note that the resistive loss is independent of the magnet length since the number of cable-to-cable connections is fixed.

The losses are expressed for a twin-aperture magnet per metre of length. The resistive loss is divided by the magnetic length of the magnets, i.e. 9 m for the PBD magnet and 13.15 m for the WBD magnet (see Table 2.1), in order to obtain a representative value of the loss in a long magnet. During a nominal field sweep the loss is dominated by the hysteresis loss, the resistive loss and, for small  $R_c$ , the ISCL. The average heat load, for a total ramp time of about 1160 s, defined as the energy loss divided by the ramp time, is about 0.37 W, which can be reduced to about 0.25 W for  $R_c > 10 \mu\Omega$ . In the case of a fast de-excitation, the main contributions are caused by the hysteresis loss and the ISCL and an initial heat load, calculated by the energy loss divided by the de-excitation time constant, of about 15 W is present, which can be reduced to 5 W for  $R_c > 10 \mu\Omega$ .

At nominal field a stationary heat-load at 1.9 K is present due to heat inleaks, resistive heating and beam-induced heating, and is estimated to be about 0.35 W per metre of cryostat [LHC, '93]. Therefore, the heat-load during the ramp to nominal field increases by a factor of about 2 compared to the stationary situation. During fast de-excitation the increase is a factor of about 40 for  $R_c=1 \mu\Omega$  and reduces to a factor of about 8 for very large  $R_c$  (so that the ISCL is almost 0).

### 6.3 Measuring losses of a magnet during ramping

The energy loss of a magnet can be measured by means of the following four methods:

- **‘Boil-off method’**. At an operating temperature around 4.2 K, the energy loss is deduced from the amount of evaporated helium during continuous field sweeps. The method is inaccurate when the helium evaporation at constant excitation is large compared to the dissipation caused by the field sweep. Another draw-back is the time needed to reach an equilibrium between the power loss and the helium evaporation. This method is applied, for example, to measure the AC loss of a 500kVA AC coil [Akita, '92].
- **‘Temperature method’**. At an operating temperature around 1.9 K, the energy dissipation during one or more field sweeps is determined from the temperature increase of the helium bath. When the amount of helium in the cryostat is large, the increase in temperature is often too small to deduce the loss accurately. The method is used to determine the loss of an LHC quadrupole magnet [Genevey, '95]. Also the loss of a toroidal pancake model is deduced by the temperature increase of the helium under forced-flow cooling [Hosono, '93].
- **‘Electrical method’**. The energy loss during a field cycle is given by the difference between the stored energy during excitation and the extracted energy during de-excitation. The method is recommended for determining the loss in superconducting magnets pulsed at low ramp rates [Gömöry, '85] and is applied for measuring the losses during ramping of SSC magnets [Ozelis, '93] and LHC magnets (see section 6.4).
- **‘Pick-up-coil method’**. The magnetisation of the coils can be determined by using pick-up coils located within the aperture, around the coils or around the collars. However, assumptions with respect to the mutual inductance between the pick-up coils and the magnetisation currents in the cable are required. A large error is likely to be present if  $R_c$  is small and varies strongly over the cross-section of the coils.

Additionally the following three methods can be used to estimate the mean time constant of the ISCCs and hence  $R_c$ :

- **‘Step-response method’**. The decay of the voltage signal over the magnet after a linear field sweep gives the time constant  $\tau_{is,M}$ . The ISCL can then be deduced since the ratio between  $P_{is,M}$  and  $\tau_{is,M}$  is constant for a given  $\dot{B}_{ce}$  and a given coil geometry (see section 6.2.3). The time constant is difficult to determine from the voltage signal when the inductive voltage is large or when the power supply is poorly regulated. The method is used to deduce the coupling loss of one LHC dipole model magnet [Tixador, '90].
- **‘Field-distortion method’**. In section 7.4 it is shown that the ratio between the dipole field  $B_{is}$ , induced by the ISCCs in the aperture of a magnet, and the average  $R_c$  is constant for a given  $\dot{B}_{ce}$ . This implies that the ISCL can be deduced from a measurement of the field distortion  $B_{is}$  during a field sweep. In chapter 7 this method is further worked out and is experimentally evaluated for several LHC dipole magnets.
- **‘Phase-shift method’**. The time constant  $\tau_{is,M}$  can be deduced from the phase shift between the current through the cable and the voltage over the cable for a sinusoidally

varying current. The results of AC loss measurements on a 500kVA AC coil using this method [Akita, '92] correspond well with the measurements using the 'boil-off method' as described above.

Here the energy loss is determined by means of the electrical method because:

- The loss of both individual magnets in the twin-aperture structure can be deduced and, therefore, also variations in the ISCL, and thus  $R_c$ , between both apertures. Also an estimate of the difference between the mean  $R_c$  in both poles of the same aperture is possible. With the 'boil-off method' and the 'temperature method' only the total energy loss of the whole magnet can be determined because both apertures are contained in the same cryostat.
- All loss components are determined, which is not possible with the 'step-response method', the 'field-distortion method' and the 'phase-shift method'.
- No assumptions have to be made about the distribution of the coupling currents over the cross-section of the magnet. The electrical method can be regarded as a measurement of the loss of a 'black box'. Independent of the location of the loss within the 'box', the loss is equal to the difference between the energy that is needed to charge the magnet and the energy that is delivered during discharging.

The hysteresis loss, the resistive loss and the total coupling loss ( $Q_{if} + Q_{is}$ ) can be separated by measuring the energy loss per cycle as a function of the central-field-sweep rate  $\dot{B}_{ce}$ . The method is similar to the one described in section 4.10.2 except that in the case of a magnet the losses  $Q_{if}$  and  $Q_{is}$  cannot be separated since the field direction in a magnet cannot be changed. Hence, the loss  $Q_{is}$  is deduced by subtracting the loss  $Q_{if}$  (calculated using  $\tau_{if}$  as determined from the magnetisation measurement) from the total coupling loss.

A measurement consists of one triangular cycle in which the central field is ramped up with a given ramp rate  $\dot{B}_{ce}$  from  $B_{ce,1}$  to  $B_{ce,2}$  and ramped down from  $B_{ce,2}$  to  $B_{ce,1}$  with  $-\dot{B}_{ce}$ . After the ramp-up and the ramp-down the transport current is kept constant for at least 50 s in order to let the ISCCs decay to zero. The energy loss of each magnet is determined during 6 to 20 triangular field sweeps with sweep rates between  $0.02 \text{ Ts}^{-1}$  and  $0.2 \text{ Ts}^{-1}$ . In order to investigate the field-dependence of the loss components, the energy loss is determined for two or more cycles with different field levels  $B_{ce,1}$  and  $B_{ce,2}$ .

The transport current  $I_{tr,cab}$  is measured by means of a current transformer (with  $U_{DCCT} = C_{DCCT} I_{tr,cab}$  with  $C_{DCCT} = 10^{-4} \text{ VA}^{-1}$ ) with a reproducibility better than  $20 \mu\text{V}$  or  $0.2 \text{ A}$ . During a field cycle the voltage  $U_{DCCT}$  and the voltage  $U_M$  over the magnet are integrated and the average current and voltage are determined during time intervals  $\Delta t$  of about  $0.3 \text{ s}$ :

$$I_{tr,cab,n} = \frac{1}{\Delta t} \int_{t_1}^{t_1+\Delta t} \frac{U_{DCCT}}{C_{DCCT}} dt \quad [\text{A}], \quad (6.19)$$

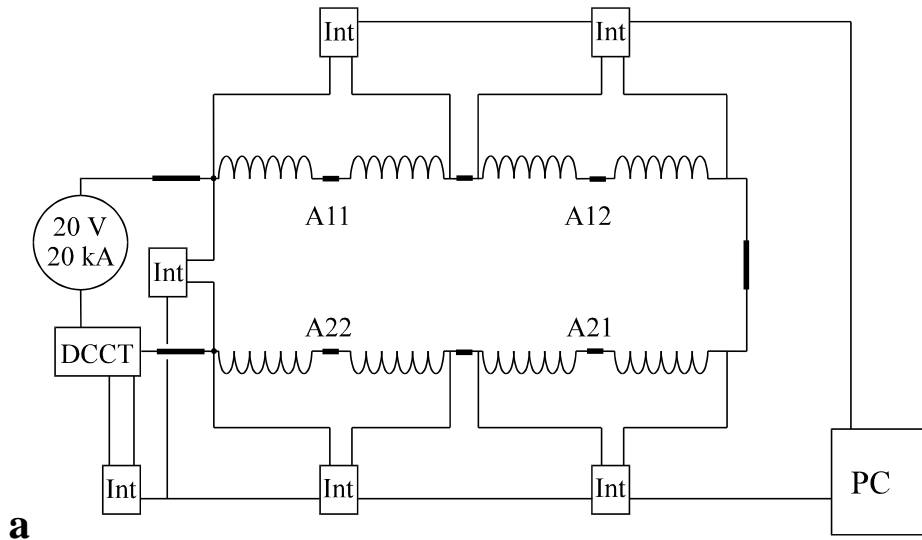
$$U_{M,n} = \frac{1}{\Delta t} \int_{t_1}^{t_1+\Delta t} U_M dt \quad [\text{V}], \quad (6.20)$$

and stored in a PC as shown in Fig. 6.4.

The loss is calculated by summation of the  $N$  incremental energies, so that:

$$Q_{tot} = \sum_{n=1}^N U_{M,n} I_{tr, cab,n} \Delta t \quad [\text{J/cycle}], \quad (6.21)$$

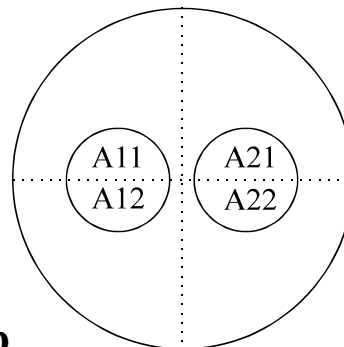
which can be regarded as the difference between the stored energy during excitation and the extracted energy during de-excitation.



**a**

**Figure 6.4.** a. The 'electrical method' for measuring losses of a superconducting magnets during field cycle between  $B_{ce,1}$  and  $B_{ce,2}$ . Simultaneously the voltages over all the four poles and the whole dipole magnet are measured.

b. Schematic view of the cross-section of a dipole magnet, indicating the nomenclature of the poles. The poles A11 and A12 form aperture 1 (or A1) and the poles A21 and A22 form aperture 2 (or A2).



**b**

The voltages over the poles are measured

simultaneously, besides the total voltage over the magnet, in order to investigate the differences in the losses between the poles. It is important that the filament magnetisation and the coupling losses, that are dissipated in the various parts of the magnet, are supplied by the magnetic field. This implies that a local energy dissipation is measured as an additional voltage in both poles and not only in the pole in which the energy is dissipated. The ratio of the voltages in both poles is related to the contribution of both poles to the local field. Energy loss near a pole results, therefore, mainly in an increase of the voltage in that pole while energy loss near the midplane results in an almost equal voltage in both poles. Only the resistive loss and the transport-current loss (i.e. the second term in eq. 6.1) are measured as a voltage over the same pole where the losses are dissipated. Hence, a difference in the measured loss between two poles cannot be carried back to a difference in  $R_c$  between the two poles since the distribution of  $R_c$  over the cross-section of the magnet is unknown. In general, the measured difference is smaller than the actual difference, since the mutual interaction between the poles causes a levelling of the loss voltages.

This effect is even more pronounced for the measured loss in the various coils of a multishell magnet. Although the loss is mainly generated in the inner coil(s), the required energy is supplied by the magnetic field which is mainly generated by the outer coil(s). So, even if voltage taps are present on the splice(s) between the various coils, the ‘electrical method’ will not reveal the actual loss in the separate coils. Of course, the same reasoning holds for the measured loss of a single block or turn.

The actual filament-magnetisation and the IFCL in the separate coils can be well estimated from short sample measurements. In the case of the ISCL,  $R_c$  is assumed to be constant all over the cross-section of the coils. The ISCL for each turn can then be determined since  $\beta_p$  (see Fig. 6.2) is known for each turn.

The accuracy of the electrical method depends on:

- The ratio between the stored energy and the energy loss during a cycle. A smaller ratio results in a more accurate loss measurement. Therefore, the energy loss can be determined more precisely by using large field-sweep rates, which increases  $Q_{tot}$ , and small fields  $B_{ce,2}$ , in order to decrease the stored energy.
- The noise and the reproducibility of the power supply.
- The time interval  $\Delta t$ . A small  $\Delta t$  results in a more accurate summation in eq. 6.21. It is possible as well to use non-integrating voltmeters with a high sampling rate. A carefully adjusted bucking coil, which compensates for the inductive component of the voltage, is preferable in order to avoid erratic results if the noise of the power supply is large.
- The drift of the voltmeters or integrators in time. Especially at small sweep rates a small drift could lead to inaccurate results. Correction for a linear drift in time is possible by performing offset measurements before and after the field cycle.

The above implies that the error of the loss measurements increases significantly for smaller field-sweep rates. This results in a relatively large error in the determination of the hysteresis loss, which is deduced from the intercept of the  $Q_{tot}-\dot{B}_{ce}$  curve at  $\dot{B}_{ce}=0$  (if the resistive loss is negligible), especially for field cycles with a large ISCL and a small hysteresis loss. Of course, performing more field cycles decreases the error in the deduction of the various loss components.

## 6.4 Experimentally determined $R_c$ -values of LHC magnets

The total energy loss of the 1 m long LHC dipole model magnets for cycles between 0 and 2 T is depicted in Fig. 6.5. This cycle is chosen in order to decrease the ratio between the stored energy and the energy loss and, therefore, to increase the accuracy. The field-sweep rate  $\dot{B}_{ce}$  varies between 0.02 and 0.2  $\text{Ts}^{-1}$ . A smaller  $\dot{B}_{ce}$  leads to a considerable increase in the relative error.

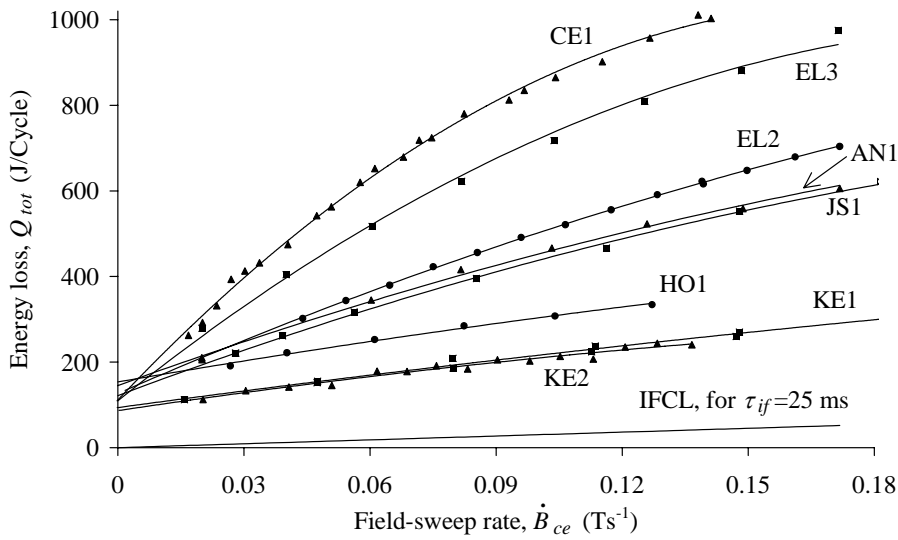


**Figure 6.5.** The energy loss per cycle and per aperture as a function of the field-sweep rate for the 1 m long dipole magnets CE1, EL3, EL2, AN1, JS1, HO1, KE1 and KE2 (from top to bottom) for a field cycle between 0 and 2 T. The solid lines represent fitting curves using eq. 6.12. The calculated IFCL is included assuming  $\tau_{if}=25$  ms.

The various loss components are evaluated by fitting the measured  $Q_{tot}-\dot{B}_{ce}$  values with eq. 6.12, neglecting the very small loss contribution from the wedges.

- The resistive loss of the connections is too small to be deduced, because the currents are small and the field-sweep rates large. Using eq. 6.15 with  $R_{tot}=2$  n $\Omega$  gives a resistive loss of about 1 J for the given field cycle at the minimum field-sweep rate of 0.02  $\text{Ts}^{-1}$ . Voltage measurements across the connections at constant transport current give an average resistance per connection of typically 0.5 to 1 n $\Omega$  (at about 5 T).
- The hysteresis loss is given by the intercept at  $\dot{B}_{ce}=0$  because the resistive loss is negligible. The error in  $Q_{hys}$  is about 10-50 J (per aperture per metre length) and is mainly due to the noise of the power supply which makes it very hard to perform accurate measurements at small field-sweep rates. As already discussed in the previous section, the error increases for magnets with a large coupling loss compared to the hysteresis loss.

- The IFCL is calculated using the  $\tau_{if}$ -values deduced from the short sample measurements (see section 3.5) in combination with eqs. 6.13 and 6.17. If  $\tau_{if}$  of a cable is not known, it is assumed to be equal to 25 ms. The IFCL corresponding to this value is also shown in Fig. 6.5, demonstrating that the IFCL makes up only a minor contribution to the total coupling losses.
- The ISCL results in an average  $R_c$  in the coil. No distinction can be made between the  $R_c$ -values of the inner and outer coils. In the case of similar  $R_c$  in both coils, the ISCL is mainly generated in the inner coil and the deduced  $R_c$  corresponds within 5% to  $R_c$  in the inner coil. No accurate  $R_c$  can be determined if the cable that is used in the outer coil has a much smaller  $R_c$  than the one used in the inner coil.

The second-order behaviour of the curves (see eq. 6.14) can be clearly seen for the magnets with a large ISCL (i.e. with a large time constant  $\tau_{is,M}$ ).

Loss measurements on the poles show that the hysteresis loss does not vary significantly among the poles, as expected since the  $J_C$ - $B$  relation of the strands of the poles are the same. An example is given in Fig. 6.6 where the loss of the four poles of the 10 m long AN2 model magnet is depicted. The relative difference between the intercepts (that is the hysteresis loss) of the four curves is less than 5%. The difference in the coupling loss between the four poles is discussed later.

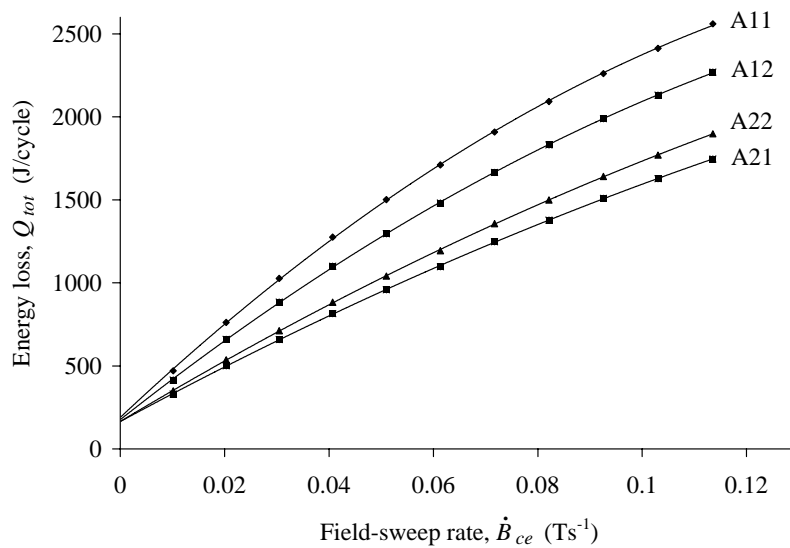


**Figure 6.6.** The energy loss in the four poles of the AN2 model magnet as a function of the field-sweep rate for a field cycle 0-2.0 T. The fitted curves (using eq. 6.12) show clearly that the four poles exhibit the same hysteresis loss whereas the ISCL varies by a factor of at least 1.5.

The results in terms of  $Q_{hys}$  and  $R_c$  for all field cycles are listed in Table 6.3. The bath temperature  $T_b$  is 1.8-2.0 K unless otherwise indicated. Only the average  $R_c$  of the whole magnet is included in the table.

**Table 6.3.** Results of the loss measurements on LHC model magnets in terms of the experimentally determined hysteresis loss  $Q_{hys,exp}$ , the calculated hysteresis loss  $Q_{hys,calc}$ , the cross-contact resistance  $R_c$  and the time constant  $\tau_{is,M}$  (calculated and deduced from a fit).

Magnet (see Table 2.3)	Cool- down	$B_{ce,1}$ T	$B_{ce,2}$ T	$Q_{hys,exp}$ J/cycle	$Q_{hys,calc}$ J/cycle	$R_c$ $\mu\Omega$	$\tau_{is,M,calc}$ s	$\tau_{is,M,fit}$ s
<b>1 m models</b>								
AN1	2	2.0	7.5	178	178	2.7	2.0	
	4	0	2.0	145	145	3.7	1.4	
	4	2.0	5.8	158	124	3.6	1.5	
CE1	2	0	2.0	144	63	1.4 (1.2 <sup>a</sup> )	3.8	4.8
	2	2.0	4.1	51	32	1.3 (1.2 <sup>a</sup> )	4.1	5.3
	2	0	3.0	139	78	1.2 (1.1 <sup>a</sup> )	4.4	
	3	2.0	6.1	135	49	1.3 (1.2 <sup>a</sup> )	4.1	
	4	0	2.0	149	64	1.7 (1.3 <sup>a</sup> )	3.1	4.1
	4	2.0	4.1	74	32	1.6 (1.4 <sup>a</sup> )	3.3	4.2
EL1	2	2.0	7.1	90	195	1.7 (1.9 <sup>a</sup> )	3.1	
	3	0	2.0	132	184	1.8	3.0	2.4
	3	2.0	6.2	184	184	1.9	2.8	
EL2	2	0	2.0	157	151	3.2	1.7	
	2 <sup>b</sup>	0	2.0	116	110	2.8	1.9	
	2	2.0	5.0	71	107	2.9	1.8	
	2 <sup>b</sup>	2.0	4.8	58	67	3.0	1.8	
	3	0	2.0	128	151	3.0	1.8	1.9
	3	2.0	5.5	113	124	3.1	1.7	1.6
	4	0	2.0	140	151	3.0	1.8	1.7
HO1	3	0	2.0	145	180	6.7	0.8	
JS1	2	2.0	7.5	65	145	3.7 (4.0 <sup>a</sup> )	1.4	
	3	2.7	7.5	113	129	3.7	1.4	
	3	2.0	8.2	145	163	3.7	1.4	
	4	0	2.0	125	130	3.6	1.5	
	5	0	2.0	109	130	3.0	1.8	1.6
KE1 <sup>c</sup>	2	0	2.0	95		6.1		
KE2 <sup>c</sup>	1	0	2.0	97		7.6		
<b>10 m models</b>								
AN2	2	0	2.0	$6.2 \cdot 10^2$	$6.5 \cdot 10^2$	1.6	3.3	3.5
	2	2.0	4.1	$3.1 \cdot 10^2$	$3.0 \cdot 10^2$	1.7	3.1	3.4
	2	0	4.1	$11 \cdot 10^2$	$9.5 \cdot 10^2$	1.6	3.3	3.5
AN3	1	0	2.0	$7.9 \cdot 10^2$	$6.5 \cdot 10^2$	6.2	0.8	
	1	2.0	4.1	$5.1 \cdot 10^2$	$3.0 \cdot 10^2$	6.8	0.7	
NO1	1	0	2.0	$6.8 \cdot 10^2$	$6.5 \cdot 10^2$	4.0	1.3	
	1	2.0	4.1	$6.8 \cdot 10^2$	$3.0 \cdot 10^2$	4.3	1.2	

<sup>a</sup>  $R_c$  determined by using the calculated hysteresis loss as a fixed point in the fit.

<sup>b</sup> Measurements performed at  $T_b = 4.3$  K.

<sup>c</sup> See [Yamamoto, '93] for more details of the different geometry. The hysteresis loss is not calculated.

The hysteresis loss is calculated numerically using the Kim relation (see eq. 2.16 with  $B_0$  and  $I_0=J_0\pi d_f^2\eta/4$  as specified in Table 3.1). The parameters  $B_0$  and  $I_0$  are assumed to be 0.31 T and  $3.0\cdot 10^{10}$  Am<sup>2</sup> for those cables which are not mentioned in Table 3.1. A linear relationship is taken between the critical current and the field for fields larger than 2-3 T (see eq. 2.18 with  $C_1=112\cdot 10^3$  A and  $C_2=7.8\cdot 10^3$  AT<sup>-1</sup>). The calculated  $Q_{hys,cal}$ -values (see Table 6.3) are in fair agreement with the experimentally determined hysteresis loss  $Q_{hys,exp}$  taking into account the error in  $Q_{hys,exp}$  and the errors in the constants as used in the  $I_C$ - $B$  relation.

The calculated hysteresis loss of the CE1 magnet is a factor 2 smaller than the measured loss. The difference is probably caused by the large coupling loss (and hence the steep slope of the  $Q_{loss}-\dot{B}_{ce}$  curve), which increases the inaccuracy in the extrapolated value for  $Q_{hys,exp}$ . The calculated hysteresis losses of one series of field cycles of the EL1 and the JS1 magnets are a factor 2 larger than the measured losses, probably caused by the large stored energy of these cycles in combination with the small number of field sweeps. For all these cycles  $R_c$  is also determined by taking the calculated hysteresis loss as a fixed point in the fit. This results in a decrease of  $R_c$  for the CE1 magnet and in an increase of  $R_c$  for the EL1 and the JS1 magnets.

The following conclusions hold with respect to the average  $R_c$  in the magnets:

- $R_c$  does not depend on the electromagnetic force on the cable and is not significantly magneto-resistive. This can be clearly seen by comparing the  $R_c$ -values deduced from field cycles at low (ca. 0-2 T) and high (up to 8 T) excitation, performed during the same cool-down.
- $R_c$  does not depend on the temperature (between 1.9 K and 4.3 K) since the ISCLs at 4.3 K and 1.9 K are equal. This is expected since no parameter that influences  $R_c$  (see section 4.3) varies significantly between 1.9 and 4.3 K.
- The average  $R_c$  of the poles differ for most of the magnets by at least 10-30%. As an example, the total losses of the four poles of the 10 m long AN2 model magnet are shown in Fig. 6.6 for a field sweep between 0 and 2 T. The average  $R_c$ -values for each aperture are about 1.3  $\mu\Omega$  for A1 and 2.0  $\mu\Omega$  for A2. Average  $R_c$ -values per pole can be calculated assuming that the loss, as measured on a pole, is generated in the same pole. This results in  $R_c$ -values of 1.2  $\mu\Omega$  (A11), 1.4  $\mu\Omega$  (A12), 2.1  $\mu\Omega$  (A21) and 1.9  $\mu\Omega$  (A22). However, the actual differences between  $R_c$  of the two poles of the same aperture are probably even larger as explained in section 6.3. This will cause larger skew harmonics during excitation of the magnets than expected from the estimated average  $R_c$  per pole (see chapter 7).

Within the accuracy of the measurement method it cannot be concluded that  $R_c$  depends on the number of cool-downs. Magnets that have been remeasured several times over a period of 2-3 years do not show any clear change in  $R_c$ .

For several series of measurements the ISCL is sufficiently large to deduce the time constant  $\tau_{is,M}$  by fitting the measurements with eq. 6.12. The time constants  $\tau_{is,M,fit}$  obtained by fitting are in good agreement with the time constants  $\tau_{is,M,calc}$  (see Table 6.3) calculated using the constant ratio between  $P_{is,M}$  and  $\tau_{is,M}$  (for a given field-sweep rate). This validates

the network model for modelling the ISCCs and the corresponding time constants in superconducting magnets.

Table 6.4 shows a brief survey of the  $R_c$ -values of all magnets arranged with respect to the cable as used in the inner coil. Although the number of magnets is too small to perform and obtain reliable statistics it can be seen that the  $R_c$ -values of different magnets made with the same cable correspond rather well for cables I-1, I-2 and I-5. Only in the case of cable I-3 is there a variation of a factor 3-4 between the magnets EL1, EL2 and HO1. This difference could originate from any of the circumstances as discussed in section 4.3. A different stress level during the curing process and different oxidation levels of the strand surface (possibly caused by the period between manufacturing the cable and winding the coil) are the most plausible causes.

**Table 6.4.** Average values of the cross-contact resistance of the inner coil for 11 LHC dipole model magnets, assuming that the  $R_c$ -values of the outer coils are of the same order or larger than those of the inner coils. TA = twin-aperture magnet, SA = single-aperture magnet.

Magnet	Type	Cable for the inner layer	Coating/soldering	$R_c$ $\mu\Omega$
AN1	1 m TA	I-1	zebra <sup>a</sup>	2.7-3.7
JS1	1 m TA	I-1	zebra <sup>a</sup>	3.0-3.7
AN2	10 m TA	I-2	SnAg	1.6-1.7
CE1	1 m TA	I-2	SnAg	1.1-1.4
EL1	1 m TA	I-3	SnAg	1.8-1.9
EL2	1 m SA	I-3	SnAg	2.8-3.2
HO1	1 m TA	I-3	SnAg	6.7
KE1	1 m SA	I-5	bare	6.1
KE2	1 m TA	I-5	bare	7.6
AN3	10 m TA	I-6	SnAg	6.2-6.8
NO1	10 m TA	I-7	SnAg	4.0-4.3

<sup>a</sup> see section 4.6

## 6.5 Conclusions

In the coils of superconducting accelerator magnets the main loss contributions are related to filament magnetisation, interfilament coupling, interstrand coupling and resistive loss. Additionally, smaller loss contributions are present in the mechanical structure, in particular the hysteresis loss in the iron yoke and the eddy-current loss in the collar pieces.

The hysteresis loss in the filaments can be directly estimated from the AC magnetisation of a single strand. The error between the measured and the calculated hysteresis loss is generally 20% and is mainly caused by the noise of the power supply which makes accurate loss measurements at small field-sweep rates very difficult. The hysteresis loss is about a factor 1.5 larger at 1.9 K compared to 4.3 K for the same field cycle. The enhancement is due to the increase of the critical current density of NbTi. The filament hysteresis is the dominant loss contribution for small central-field-sweep rates of the order of  $10^{-2} \text{ Ts}^{-1}$  and weak-field excitation.

For larger field-sweep rates or strong field excitations the coupling losses dominate. The IFCL and the ISCL of a magnet can be separated once the IFCL of a strand or cable is known. In the LHC dipole model magnets the ISCL is at least a factor 10 larger than the IFCL and is mainly generated in the inner coil near the midplane. While the IFCCs are characterised by a time constant of about 25 ms, the ISCCs exhibit time constants of about 1 to 5 s, attributed to a small contact resistance  $R_c$  between crossing strands of about 1 to 8  $\mu\Omega$ . The effect of such small  $R_c$  on the field homogeneity and temperature margin during ramping is discussed in chapters 7 and 8.

The experimentally deduced time constants of the ISCCs correspond well with calculated values using the network model in combination with the determined  $R_c$ -values. This validates the use of the network model to calculate the ISCCs and their time constants in superconducting magnets.

The eddy-current losses in the copper wedges and collar pieces are small compared to the coupling losses in the cable and the magnetisation loss in the iron yoke is small compared to the magnetisation loss in the filaments.

Experimental results on LHC dipole model magnets show that the  $R_c$ -values of cables with SnAg-coated strands:

- are temperature-independent (between 1.9 K and 4.3 K),
- vary by a factor of up to 1.5 between the two poles of the same aperture,
- do not depend on the field level and therefore do not significantly depend on the Lorentz force on the cable and on the matrix resistivity.

Three magnets in which the same cable is used have been shown to exhibit an ISCL which differs by a factor 3-4. The difference in  $R_c$  is probably due to different stress levels (during curing) and surface conditions of the strands between the models. Three other cables are all used in two magnets. No large differences in  $R_c$  between the two magnets are observed for these cables.

The energy dissipation during a nominal field sweep from 0.6 to 8.4 T is dominated by the hysteresis loss, the resistive loss and, for small  $R_c$ , the ISCL and is about 450 J (for  $R_c=2 \mu\Omega$ ) per metre for a twin-aperture magnet (see Table 6.2). The average heat-load is about 0.38 W for excitation in about 20 minutes. A fast de-excitation, with a de-excitation time constant of 100 s, leads to an energy dissipation of about 1500 J (for  $R_c=2 \mu\Omega$ ), mainly caused by the hysteresis loss and the ISCL, and consequently an average heat load of 15 W. If  $R_c > 10 \mu\Omega$ , the average heat load can be reduced to 0.25 W for a nominal field sweep and 5 W for a fast de-excitation.

The losses in superconducting accelerator magnets during ramping can be well determined by means of the ‘electrical method’, based on the measurement of the difference between the stored energy and the extracted energy during a field cycle. The method is relatively fast and accurate, especially for field cycles at low excitation levels where the stored energy is small. The hysteresis loss and coupling losses can be well distinguished with an accuracy that is mainly limited by the noise and the regulation of the power supply.